scientific reports

Check for updates

OPEN

Correlation of optic nerve hemoglobin levels with structural and functional parameters in glaucoma

Gustavo Coelho Caiado, Gustavo Albrecht Samico, Gilvan Vilarinho da Silva Filho, Sergio Henrique Teixeira, Tiago Santos Prata, Carolina Pelegrini Barbosa Gracitelli & Augusto Paranhos Jr.✉

Glaucoma is a chronic and progressive eye disease that leads to irreversible damage to the optic nerve and retinal nerve fiber layer, resulting in visual field loss. Abnormalities in retinal blood flow and vascular regulation are increasingly recognized as key factors in glaucoma development. This study explores the relationship between optic nerve head hemoglobin (ONH Hb) levels, assessed through automated colorimetric analysis using Laguna ONhE software, and structural and functional parameters in glaucoma patients. The study included 57 glaucoma patients (89 eyes) and evaluated correlations between ONH Hb levels, retinal nerve fiber layer thickness (RNFLT), ganglion cell layer thickness (GCLT), foveal avascular zone (FAZ) metrics, and visual field indices. Results showed significant correlations between ONH Hb levels and visual field mean defect, RNFLT, and GCLT, highlighting the potential of ONH Hb as a non-invasive marker for glaucoma-related structural changes. The findings suggest that ONH Hb assessment could serve as a practical and cost-effective tool for glaucoma diagnosis and monitoring, particularly in settings where advanced imaging technologies like OCT and OCTA are less accessible. This study underscores the importance of vascular factors in glaucoma and supports the use of ONH Hb evaluation as a complementary approach to traditional diagnostic methods.

Keywords OCT angiography, Glaucoma, Foveal avascular zone, Perimetry, Laguna ONhE software

Glaucoma is a chronic, progressive and potentially blinding eye disease that causes irreversible damage to the optic nerve rim and retinal nerve fiber layer (RNFL) leading to visual field defects[1]. Despite the availability of the diagnostic and therapeutic options, many patients remain undiagnosed or continue to experience disease progression[2]. Impairment of ocular blood flow may play a significant role in the prevalence and development of glaucoma[3–5]. Techniques such as optical coherence tomography angiography (OCTA) have been developed to measure vascular integrity and blood flow[6].

The idea that tissue perfusion and oxygenation and hemoglobin (Hb) levels are related has been examined in earlier research[7]. Well-perfused tissues exhibit adequate Hb levels, while lower levels are associated with tissue loss[8,9]. Impaired blood flow, leading to tissue hypoxia, has been associated with retinal ganglion cell loss[8,10]. In the optic nerve head (ONH), the levels of hemoglobin indicate the vascular supply that supports the axons of retinal ganglion cells and glial cells[8]. Macular damage and optic nerve lesion staging are linked in glaucoma, with nerve loss often corresponding to macular ganglion cell damage[11–13]. Vascular changes in the macula, common in glaucoma, may indicate broader blood flow issues[14,15]. Therefore, studying optic nerve head hemoglobin via could provide insights into these vascular and structural changes.

A straightforward technique to measure hemoglobin levels in the optic nerve head (ONH) involves evaluating standard retinography using automated colorimetric analysis with using software Laguna ONhE[16–19]. Some studies have demonstrated that lower levels of optic nerve head hemoglobin (ONH Hb) are found in patients with established glaucoma, along with high reproducibility results, good diagnostic capability, and diagnostic agreement with other morphologic procedures, both in glaucomatous and nonglaucomatous eyes[9,16,20,21]. Deep

Department of Ophthalmology and Visual Science, Glaucoma Service, Federal University of São Paulo, Rua Botucatu, 821, Vila Clementino, São Paulo CEP: 04023-062, Brazil. ✉email: augusto.paranhos@gmail.com

learning methods for the segmentation of optic nerve edges were incorporated to facilitate its use and improve its reproducibility[20].

Considering all the aforementioned aspects, the purpose of this present study was to evaluate the structure/structure and structure/function associations using levels of ONH Hb, assessed by automated colorimetric analysis, and RNFL thickness (RNFLT), ganglion cell layer thickness (GCLT), central macular vessel density (VDm), foveal avascular zone (FAZ) metrics (area, perimetry and circularity) and visual field indices (Mean defect and Mean sensitivity) in glaucoma subjects.

Materials and methods

Study population

This cross-sectional study of glaucoma subjects was approved by the Ethics Committee of Federal University of São Paulo (Ethics Committee Approval Number: 35713820.2.0000.5505) and was conducted in accordance with the tenets of the Declaration of Helsinki. Written informed consent was obtained from all participants. Glaucomatous subjects were recruited from glaucoma division from Ophthalmology and Visual Sciences Department at Federal University of São Paulo. Patients with glaucoma were enrolled in the study based on clinical findings consistent with glaucomatous optic neuropathy, such as vertical cup-to-disc ratio > 0.6, asymmetry of cup- to-disc ratio > 0.2 between eyes, and presence of localized RNFL or neuroretinal rim defects corresponding to abnormal visual field (VF) in standard automated perimetry (SAP) in the absence of any other abnormalities that could explain the findings on fundus examination[22]. Abnormal visual field was defined as follows[23]: (1) outside normal limit on glaucoma hemifield test or (2) three abnormal points with *P* less than 5% probability of being normal or one abnormal point with *P* less than 1% by pattern deviation, or (3) pattern standard deviation (PSD) of 5% if the VF was otherwise normal, confirmed by two consecutive tests. A VF measurement was considered to be reliable when false-positive results were less than 15%, false-negative results were less than 15% and fixation losses were less than 20%. There was no washout period before the exams due to the severity of the glaucomatous damage. IOP was recorded while the patients were using their antiglaucoma medications and was measured on the day of the exams.

All participants underwent a comprehensive ophthalmic examination, which included assessment of visual acuity, IOP measurement by Goldmann applanation tonometry, slit lamp examination of the anterior segment, fundoscopy, gonioscopy, axial length measurement by optical (IOL Master 500, Carl Zeiss Meditec, Dublin, CA) and swept-source OCT and OCTA (DRI OCT Triton, Topcon Inc, Tokyo, Japan) examination. We used the same DRI OCT instrument to perform OCT and OCTA scans. Patients underwent standard VF examination by the static automated white-on-white Macular and G Program (Octopus 900, Haag-Streit, AG, Koeniz, Switzerland).

Exclusion criteria included the following: (1) participants aged under 18 years and older than 80 years; (2) a spherical equivalent within +3 to −6 diopters; (3) best corrected visual acuity > 1.0 logMAR; (4) non-glaucomatous optic neuropathy and retinopathy, previous or active uveitis, hypertensive retinopathy, diabetic retinopathy, age-related macular degeneration, pathological myopia with epiretinal membrane, macular hole, retinal detachment or ocular trauma; (5) neurodegenerative diseases such as Parkinson's or Alzheimer's diseases, (6) history of stroke; (7) any other known disease that may cause optic neuropathy, retinopathy or VF loss; (8) an unreliable VF; (9) poor-quality OCTA scans as described later.

OCT and OCT-A imaging acquisition

All subjects were examined using the macular 4.5 × 4.5 mm scanning protocol (DRI OCT Triton; Topcon Corporation, Tokyo, Japan). Topcon OCTA instrument uses a wavelength of 1050 nm with A-scan rate of 100,000 scans per second. The instrument produces maps using OCTA ratio analyses (OCTARA), which is an amplitude-decorrelation ratio-based algorithm[24]. The system automatically divided the macula into four layers, and the selected layer was superficial retinal capillary plexus (SCP). The SCP is defined as from the inner border of the retinal nerve fiber layer to 15.6 µm from the boundary between the inner plexiform layer and the inner nuclear layer. FAZ, VDm, mean RNFLT and mean GCL + thickness (mean GCLT) were evaluated using Triton OCTA. VDm, mean RFNLT and mean GCLT were automatically measured by OCTA. Vascular parameters were: FAZ area, perimeter and circularity as also VDm. Structural parameters were mean RNFLT and mean GCLT.

OCT-A images with poor image quality or significant image artifacts were excluded before the quantitative analysis, including: (1) image quality score less than 40, (2) inaccurate segmentation of tissue layers, (3) motion artifacts (e.g., vessel discontinuity) or slabs, (4) blurry images, (5) poor centration or (6) signal loss (e.g., due to eye blinking).

OCT-A imaging processing: FAZ segmentation and quantification

The area was defined as the size of the segmented FAZ region, and the perimeter was determined by the length of the FAZ contour. The circularity was then calculated as an index using the formula where circularity = 4π (area/perimeter^2), indicating the compactness of shape relative to a circle. A ratio closer to 0 indicates a more irregular shape far away from a circle[25]. In ImageJ, the measurement results were shown in pixel units. Because the images for the 4.5 mm × 4.5 mm protocol exported from the OCT were 719 × 719 pixels, the unit of pixel was converted to millimeters at a ratio of 719 to 4.5.

The Level Sets Macro (LSM) was used as it LSM exhibited greater accuracy and reliability compared to the KSM and inbuilt automated methods[25]. It is a plugin utilizing the theory of partial differential equations that can progressively compare pixel differences with neighboring pixels and converge at the boundary where the differences are the highest (available at https://imagej.net/Level_Sets). After importing the 8-bit grayscale image into ImageJ, inserting an oval to act as an initial seed inside the FAZ is required before running the program (Fig. 1a). The shape and the size of the initial seed are not particularly important, but it is essential that the seed

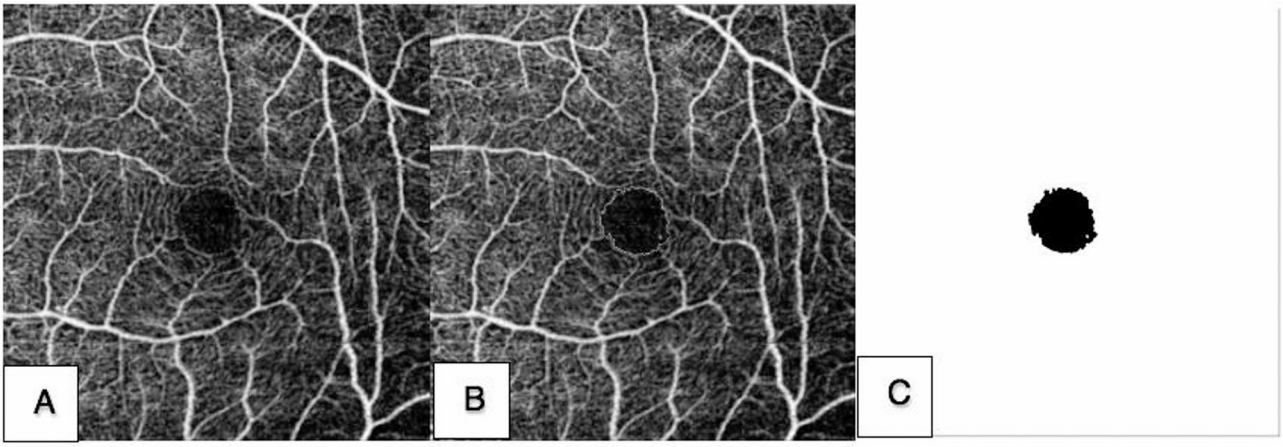

Fig. 1. Procedure for FAZ segmentation by the LSM. (**a**) An initial seed at the center of the FAZ is required. (**b**) After running the LSM, the contour advances and can be viewed in the processing window. (**c**) When it hits the boundary, the FAZ segmentation is finished.

be entirely inside the FAZ, preferably located at the center of the FAZ. Based on the optimized parameters, the contour advances and can be viewed in the progress window (Fig. 1b). When the contour hits the boundary, segmentation of the FAZ is finished (Fig. 1c). Finally, the LSM automatically measures and outputs the FAZ metrics (area, perimeter, and circularity)[25].

The parameters of the LSM were optimized as follows. The Active Contours method was chosen for the LSM rather than Fast Marching because the latter method is prone to leaking, especially when there is a gap at the FAZ boundary. This program advances the contour like a rubber band, with the strength being controlled by the nature of the curvature. The convergence serves as the convergence criterion and compares the changes in contour between two iterations. We used the grayscale of 30 as it performed better compared to other values[25].

The area (A_{imagej}) calculated using ImageJ were adjusted for ocular magnification considering axial length of each eye. The adjusted FAZ area ($A_{adjusted}$) (in mm2) was then calculated as follows: $A_{adjusted} = A_{imagej}$ (ALs/ALm)^2, where ALs is the axial length of the subject in mm, and ALM is the axial length assumed for the model eye by the manufacturer (24.39 mm) (DRI OCT Triton, Topcon Inc, Tokyo, Japan).

Visual field assessment

Octopus 900 (Octopus 900, Haag-Streit, AG, Koeniz, Switzerland), white-on-white perimeter was used to evaluate VF of glaucoma patients. G and Macular program were used. The G program has a physiology-based grid of 59 test locations within the central 30 degrees. Locations are clustered more closely together centrally (2.8 degree spacing) with five central foveal locations and 17 test locations in the macular region. Locations are spaced further apart peripherally with emphasis on locations in nasal step regions and with more test locations nasally than temporally. Macular program consists in 45 points one degree spacing in the fovea (central 4 degrees) and 36 points radially oriented from 4 to 10 degrees. Goldmann size III stimuli against a photopic background luminance of 31.4 apostilbs (10 cd/m^2), TOP strategy, white-to-white, were used. A VF measurement was considered to be reliable when false-positive results were less than 15%, false-negative results were less than 15% and fixation losses were less than 20%. VF variables analysed were mean defect (MD) and mean sensitivity (MS).

Color fundus imaging processing

The color fundus retinography was analysed by Laguna ONhE software. A detailed description of the use of the program has been published[16]. In brief, Laguna ONhE utilizes conventional fundus photographs to quantify the ONH Hb level. The software evaluates three spectral components of ONH images: red, green and blue. The red component is linked to ONH areas with high Hb concentration. Conversely, regions with low Hb content reflect a smaller proportion of red light compared to green and blue components. The analysis of various formulas, which are determined by the reflected levels of red, green, and blue light, exhibited an almost linear relationship with the Hb level[16]. The limits of Bruch' s membrane was not taken into account to delimit the edges of the ONH when using the Laguna ONhE program. However, the automatic edge identification algorithms used by this program take into account the experience accumulated in other studies in which the photographic images were adjusted with the ONH edges delimited by OCT[19].

The technique employs multiple convolutional neural networks to detect the optic nerve and its boundaries, locate the inner edge of the Elschnig scleral ring, assess the image quality, determine the eye's laterality, segment the vessels, and analyze their patterns. The deep learning neural network responsible for evaluating image quality is programmed to exclude abnormal optic discs, such as myelin fibers within the optic disc, myopic gyrate atrophies, optic disc edema, and colobomas[16,18,20]. Other algorithms play a crucial role in identifying whether an image has been enlarged and in estimating the areas of the disc, cup, and rim sectors. The nerve tissue is also evaluated through colorimetry against the vessels of the central retinal artery and its vein branches, which are utilized as a benchmark. The relationship established between these components aids in estimating

the presence of hemoglobin in various regions of the optic disc. Additionally, the relationships between the size and shape of the cupping, adjusted for the optic disc size, along with other factors such as the presence of peri-papillary atrophies, are integrated into two principal indices: the globin or glaucoma discriminant function (GDF), where the deep learning classifier for glaucoma versus normal conditions exerts considerable influence, with a range of approximately − 100 to + 85 units, and the globin individual pointer (GIP), which focuses more on the specific characteristics of the individual's nerve, allowing for the detection of temporal changes due to its superior reproducibility, with a range of around − 100 to + 100[26]. When inputting PSD or sLV (square root of loss variance) data, it generates a GDF PSD index. GDF glaucoma when the value is below − 15 with a specificity of 99%[27]. The method shows excellent intraobserver, interobserver, within-session and between-session reproducibility in pseudophakic patients with and without glaucoma along with high interanalysis reproducibility when performed by a masked examiner[9,26,27].

The optic disc size is automatically measured using deep learning-based segmentation of retinal images[27,28]. A neural network (U-Net) precisely identifies the disc boundaries by detecting Elschnig's scleral ring, achieving excellent accuracy (as evidenced by a Sørensen-Dice similarity index of 0.993 when compared to manual segmentations, demonstrating near-perfect agreement with human expert delineations)[27,28]. The area is calculated by counting pixels within these boundaries and converting them to mm^2 using a standardized reference (median 1.95 mm^2 from OCT data)[27,28]. This method accounts for different cameras and zoom levels while maintaining high consistency (average 0.01 mm^2 variation between devices)[27,28]. Though it doesn't adjust for refractive errors, it reliably classifies discs as small or large relative to population norms[27,28]. The measurements show strong correlation ($R = 0.953$) with OCT-based tissue thickness when combined with hemoglobin perfusion analysis[27,28]. Validated with good reproducibility (ICC 0.984), this automated approach provides standardized disc size measurements valuable for glaucoma diagnosis and large-scale studies, integrating well with other diagnostic parameters for comprehensive optic nerve assessment[27,28].

Figure 2 demonstrates an example of a patient with glaucomatous ONH and the respective pseudo-images indicating the Hb levels. The software provides an index called GDF, which combines the results of total Hb and relative Hb obtained in various sectors of the optic nerve to differentiate between glaucoma and normality. This index divides the ONH into 3 concentric rings, each divided into 8 parts, totaling 24 sectors[16]. GDF which combines the Hb slope, obtained through multiple regression analysis of Hb estimated for each sector with the mean Hb amount determined in the vertical disc diameter, in sectors 8 and 20. ONH Hb is expressed as a percentage (%). GDF is expressed as a whole number from + 75 to -90. It describes the probability that the optic nerve disc shows an Hb amount within the normal range (positive values) or in the range consistent with glaucoma (negative values). The relationship is therefore direct such that the further the GDF from zero in either direction, the greater the likelihood will be that the disc belongs to one or the other diagnostic groups[9].

The outer ring mostly aligns with the neuroretinal rim, the central ring corresponds to the transition area, which may include the neuroretinal rim and cupping, and the inner rim mainly comprises the cup area. As with other imaging techniques used in glaucoma diagnosis, this alignment can be more difficult in tilted discs. On the basis of colorimetric analysis of the papilla, it is known that both in control individuals and in patients with glaucoma, Hb levels are greater in the more peripheral sectors, that is, in the outer ring. The middle ring tends to show a lower amount of Hb than the outer ring, and the innermost ring features the least amount of Hb. In other words, tissue Hb levels diminish from the disc periphery towards the center such that the difference between peripheral and central Hb levels can be calculated. By determining color changes in the central disc zone, the software estimates the cup and cup–disc ratio[9].

All images that did not pass the quality control of the Laguna ONhE program or images of poor quality due to media opacity or inadequate focus were excluded.

Statistical analysis

The Shapiro-Wilk test was used to evaluate the distribution of the variables. Among those included in the regression model, only the variables related to the visual field were not normally distributed. A regression analysis using mixed linear models was performed to account for the dependence between the two eyes of the same patient. In this model, the patient was included as a random effect, allowing the natural correlation between intra-individual ocular measurements to be considered and enabling more accurate estimation of the fixed effects of interest. The results are presented as R^2 values, similar to those used in conventional linear models. Univariate and multivariate analyses were performed.

Laguna parameters (GDF, GIP and GDF PSD) were treated as dependent variables, while RNFLT, FAZ metrics, VDm and GCLT were considered independent variables for structure/structure analysis. For structure/function analysis VF parameters (MD for G program (MDg), MD for Macular program (MDm) and MS for Macular program (MSm)) were the dependent variables, with RNFLT, FAZ metrics, VDm and GCLT as independent variables.

All statistical analysis were performed using the available software IMB SPSS Statistics version 29.0.2.0. and JAMOVI (version 2.4.7.0). The alpha level (type I error) was set as 0.05.

Results

89 eyes of 57 glaucoma patients (30 female and 27 male) were included in this study. The mean age was 66.67 ± 7.49 years old. The mean MDg was 7.91 ± 7.18 dB. The mean of GDF, GIP, GDF PSD, MDm, GCLT and NFL thickness and FAZ parameters were described in Table 1.

For function/structure analysis, significant associations were found between Laguna ONhE parameters and visual field indices. MDm was significantly correlated with GDF ($p < 0.001$; $R^2 = 0.117$), GDF PSD ($p < 0.001$; $R^2 = 0.170$) and GIP ($p = 0.002$; $R^2 = 0.104$). MSm was significantly associated with GDF ($p < 0.001$; $R^2 = 0.116$), GDF PSD ($p < 0.001$; $R^2 = 0.171$) and GIP ($p = 0.002$; $R^2 = 0.103$). MDg was significantly correlated with GDF

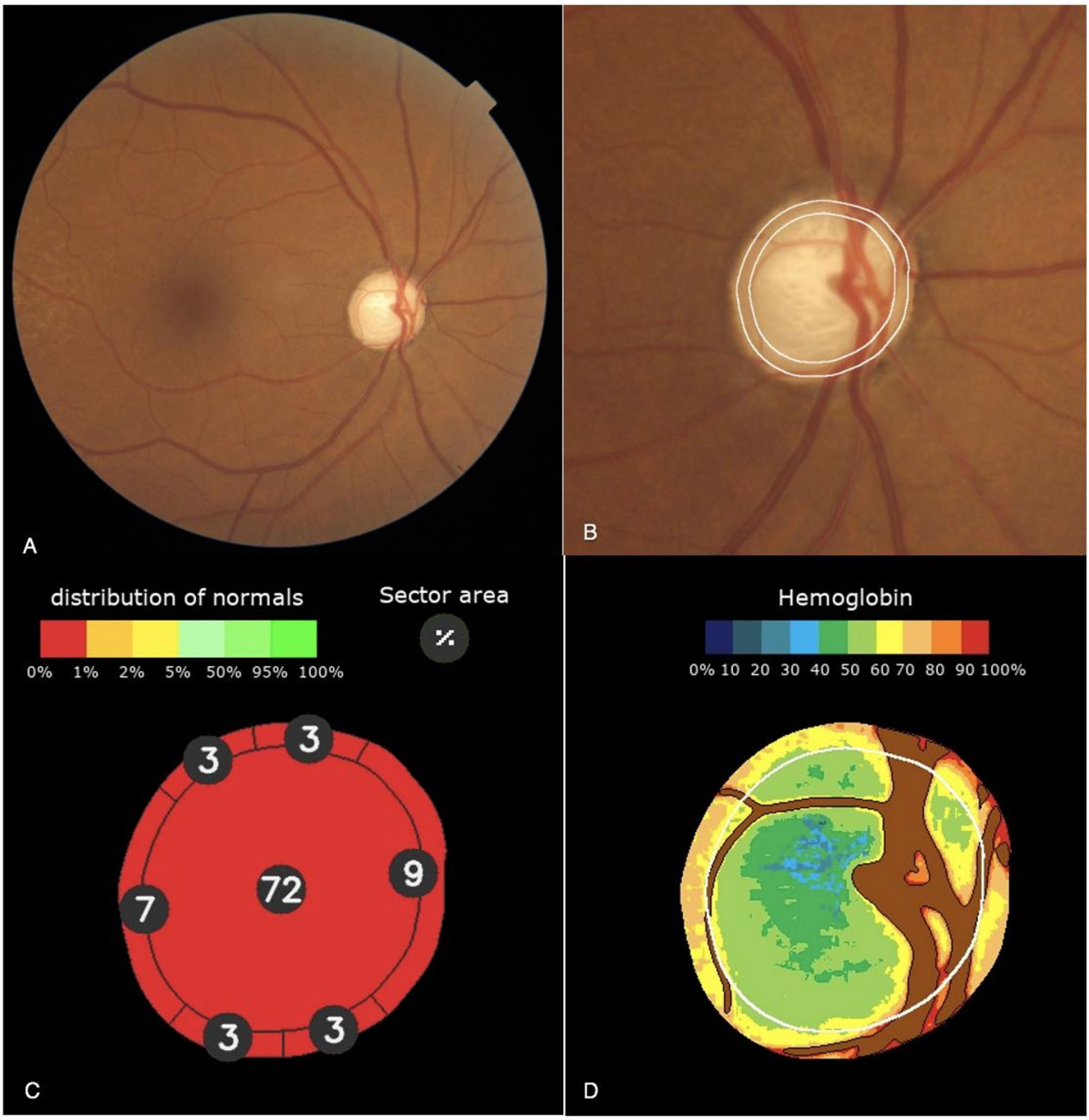

Fig. 2. Example of Laguna ONhE analysis: (**a**) Original wide-field eye fundus image. (**b**) Identification of the optic disc and boundaries segmentation. Central cup estimated from the hemoglobin distribution. (**c**) Estimated sector areas as a percentage of the total area and compared to a normal reference population. (**d**) Segmentation of reference vessels and pseudo-color image of hemoglobin distribution.

($p < 0.001$; $R^2 = 0.212$), GDF PSD ($p < 0.001$; $R^2 = 0.339$) and GIP ($p < 0.001$; $R^2 = 0.167$). sLV of M program was significantly associated with GDF ($p < 0.001$; $R^2 = 0.233$), GDF PSD ($p < 0.001$; $R^2 = 0.414$) and GIP ($p < 0.001$; $R^2 = 0.164$). sLV of G program was significantly associated with GDF ($p < 0.001$; $R^2 = 0.237$), GDF PSD ($p < 0.001$; $R^2 = 0.603$) and GIP ($p < 0.001$; $R^2 = 0.174$). For structure/structure analysis, significant associations were found. Mean GCLT was significantly correlated with GDF ($p < 0.001$; $R^2 = 0.173$), GDF PSD ($p < 0.001$; $R^2 = 0.187$) and GIP ($p < 0.001$; $R^2 = 0.200$). Mean RNFLT was significantly correlated with GDF ($p < 0.001$; $R^2 = 0.386$), GDF PSD ($p < 0.001$; $R^2 = 0.498$) and GIP ($p < 0.001$; $R^2 = 0.319$). VDm did not show significant correlation with GDF ($p = 0.695$; $R^2 = 0.002$), GDF PSD ($p = 0.454$; $R^2 = 0.006$) and GIP ($p = 0.981$; $R^2 = 0.000$). FAZ area was only significantly associated with GIP ($p = 0.017$; $R^2 = 0.078$). FAZ perimeter was not significantly correlated with GDF ($p = 0.182$; $R^2 = 0.020$), GDF PSD ($p = 0.333$; $R^2 = 0.009$) and GIP ($p = 0.107$; $R^2 = 0.029$). FAZ circularity did not show significant correlation with GDF ($p = 0.267$; $R^2 = 0.014$), GDF PSD ($p = 0.431$; $R^2 = 0.007$) and GIP

	Glaucoma patients ($n=57$) Mean ± SD
Age (years)	66.67 ± 7.49
Sex (male)	27
GIP (Laguna ONhE)	− 45.7 ± 42.9
GDF (Laguna ONhE)	− 39.7 ± 31.0
GDF PSD (Laguna ONhE)	− 32.2 ± 17.8
Axial length (mm)	23.6 ± 1.18
Mean MDm (dB)	5.59 ± 6.26
Mean MDg (dB)	7.91 ± 7.18
sLV M program (dB)	4.03 ± 2.36
sLV G program (dB)	4.48 ± 2.01
Mean central GCLT (µm)	56.30 ± 6.95
Mean RNFLT (µm)	75.60 ± 22.90
Mean central VDm (%)	12.9 ± 0.89
Mean FAZ area (mm^2)	0.431 ± 0.159
Mean FAZ circularity	0.387 ± 0.130
Mean FAZ perimeter (mm)	4.02 ± 1.1

Table 1. Clinical characteristics of the study sample. *GDF* glaucoma discriminant factor, *GDF PSD* glaucoma discriminant factor + patterns standard deviation, *GIP* globin individual pointer, *MDm* mean defect of macular program, *MDg* mean defect of G program, *sLV* square root of loss variance, *GCLT* ganglion cell layer thickness, *RNFLT* retinal nerve fiber layer thickness, *FAZ* foveal avascular zone, *VDm* macular vessel density.

	GDF		GDF PSD		GIP	
	R^2	*P* value	R^2	*P* value	R^2	*P* value
MDm (dB)	0.117	< 0.001	0.170	< 0.001	0.104	0.002
MSm (dB)	0.116	< 0.001	0.171	< 0.001	0.103	0.002
MDg (dB)	0.212	< 0.001	0.339	< 0.001	0.167	< 0.001
sLV (M program)	0.233	< 0.001	0.414	< 0.001	0.164	< 0.001
sLV (G program)	0.237	< 0.001	0.603	< 0.001	0.174	< 0.001
VDm (%)	0.002	0.695	0.006	0.454	0.000	0.981
Mean GCLT (µm)	0.173	< 0.001	0.187	< 0.001	0.200	< 0.001
Mean RNFLT (µm)	0.386	< 0.001	0.498	< 0.001	0.319	0.001
FAZ area (mm^2)	0.046	0.069	0.029	0.136	0.078	0.017
FAZ perimeter (mm)	0.020	0.182	0.009	0.333	0.029	0.107
FAZ circularity	0.014	0.267	0.007	0.431	0.001	0.744
Brusini's staging system	0.270	< 0.001	0.469	< 0.001	0.196	0.002

Table 2. Correlations between Laguna ONhE parameters and functional and structure parameters. *GDF* glaucoma discriminant factor, *GDF PSD* glaucoma discriminant factor + pattern standard deviation, *GIP* globin individual pointer, *MDm* mean defect of macular program, *MSm* mean sensitivity of macular program, *MDg* mean defect of G program, *sLV* square root of loss variance, *VDm* macular vessel density, *GLCT* ganglion cell layer thickness, *RNFL* retinal nerve fiber layer thickness, *FAZ* foveal avascular zone.

($p=0.744$; $R^2=0.001$). Brusini`s staging system was significantly correlated with GDF ($p<0.001$; $R^2=0.270$), GDF PSD ($p<0.001$; $R^2=0.469$) and GIP ($p=0.002$; $R^2=0.196$). All the associations were described in Table 2.

Discussion

Comprehensive understanding of the structure-function and structure-structure relationship in individuals with glaucoma is crucial for accurate diagnosis and effective disease management[29,30]. Increasing attention has been paid directed toward the role of abnormal intraocular blood flow and impaired vascular regulation in the development and progression of various types of glaucoma[31–34]. The advancements in OCT and OCTA imaging technology have significantly contributed to the objective evaluation of structural changes[35,36]. Nevertheless, the application of OCT and OCTA may be constrained in specific clinical cases due to intrinsic ocular features or technical obstacles (tilted discs, advanced glaucoma, peripapillary atrophies, or high myopia)[37–39]. Moreover, their elevated cost hinders universal application for a disease with such high prevalence[40,41]. It is therefore important to assess the cost/benefit ratio of diagnostic and monitoring methods, and methods less influenced by anatomic variables[41].

Laguna ONhE is a noninvasive method that is not expensive to measure hemoglobin levels as it is performed on retinal photographs and thus only a fundus camera is needed[9]. Previous studies have demonstrated that this method has good sensitivity and specificity[21,22,26,42]. Meneses et al.[42] reported that GDF yielded 79.3% sensitivity at a fixed specificity of 95% ($p < 0.001$, AUC 0.93). Mendez-Hernandez et al.[9] evaluated Laguna ONhE parameters and obtained all ICC values above 0.8 indicating good reproducibility. Therefore, evaluate Laguna ONhE indices and its correlations may play an important role in glaucoma diagnosis and progression. In our study, we found a significant correlation between Laguna ONhE parameters and perimetry field indices (MDm, MSm and MDg). Regarding structure/structure evaluation, Laguna ONhE indices were significantly correlated with mean GCLT and mean RFNLT. In addition, FAZ area was significantly associated with GDF, GDF PSD and GIP. FAZ perimeter and FAZ circularity were not significantly correlated with GIP, GDF and GDF PSD. Figure 3 demonstrates exams of a glaucoma patient from our study.

Limited data in the literature exist regarding structure-structure correlations using Laguna ONhE indices[16,17,21,22,43]. In our study, mean RFNL were significant moderate correlated with GDF ($R^2 = 0.386$, $p < 0.001$) and GDF PSD ($R^2 = 0.498$, $p < 0.001$). We also found that mean GCLT was significantly correlated with GDF ($p < 0.001$; $R^2 = 0.173$), GDF PSD ($p < 0.001$; $R^2 = 0.187$) and GIP ($p < 0.001$; $R^2 = 0.200$). The literature is consistent with our results. Rocha et al.[22] found significant linear correlation between GDF and RNFLT values ($R^2 = 0.195$, $p < 0.001$). Gonzalez-Hernandes et al.[17] observed that GDF index had a very high correlation with the mean thickness of the RNFL (R2 = 0.85, $p < 0.001$) and the thickness of the neuroretinal rim in the ONH itself ($R^2 = 0.81$, $p < 0.001$) and also found a significant correlation between anatomical damage (RNFL thickness) and hemoglobin content in specific sectors of the ONH. Gonzalez de la Rosa et al.[16] and Mendez-Hernandez et al.[21], demonstrated a significant association between the GDF index and OCT parameters along with perimetry results ($p < 0.001$). Mendez-Hernandez et al.[21] also observed that the correlations between GDF and RNFLT values for the nasal and temporal quadrants were low while higher correlation was observed at the vertical meridian (GDF showed greatest correlation with RFNLT in the inferior sector, $R^2 = 0.622$; $p < 0.001$). This could be due to the important role played by the vertical disc quadrants in glaucoma as the GDF is based on Hb levels in these sectors[21]. Regarding vascular parameters, the only significantly association was found between FAZ area and GIP ($p = 0.017$; $R^2 = 0.078$). VDm did not show significant correlation with GDF ($p = 0.695$; $R^2 = 0.002$), GDF PSD ($p = 0.454$; $R^2 = 0.006$) and GIP ($p = 0.981$; $R^2 = 0.000$). Mendez-Hernandez et al.[44] found significant correlations between vessel density measured by OCTA and GDF. They found significant moderate correlation between GDF and circumpapillary vessel density (p = < 0.001; $R^2 = 0.570$), GDF and optic nerve head vessel density (p = < 0.001; $R^2 = 0.574$), and GDF and macular vessel density (p = < 0.001; $R^2 = 0.397$)[46].

Studies have shown structure-function association between Laguna ONhE and visual field mean deviation. In our study, MDm was significantly correlated with GDF ($p < 0.001$; $R^2 = 0.117$), GDF PSD ($p < 0.001$; $R^2 = 0.170$) and GIP ($p = 0.002$; $R^2 = 0.104$). MSm was significantly associated with GDF ($p < 0.001$; $R^2 = 0.116$), GDF PSD ($p < 0.001$; $R^2 = 0.171$) and GIP ($p = 0.002$; $R^2 = 0.103$). MDg was significantly correlated with GDF ($p < 0.001$; $R^2 = 0.212$), GDF PSD ($p < 0.001$; $R^2 = 0.339$) and GIP ($p < 0.001$; $R^2 = 0.167$). sLV of M program was significantly associated with GDF ($p < 0.001$; $R^2 = 0.233$), GDF PSD ($p < 0.001$; $R^2 = 0.414$) and GIP ($p < 0.001$; $R^2 = 0.164$). sLV of G program was significantly associated with GDF ($p < 0.001$; $R^2 = 0.237$), GDF PSD ($p < 0.001$; $R^2 = 0.603$) and GIP ($p < 0.001$; $R^2 = 0.174$). The literature is consistent with our results. Rocha et al.[22] observed significant nonlinear and weak correlation between GDF and visual field mean deviation (VFMD) ($R^2 = 0.295$, $p < 0.001$). Medina-Mesa et al.[19] observed a linear moderate correlation between mean deviaton and the amount of Hb in the superior and inferior sections of the rim ($R^2 = 0{,}401$, $p < 0.001$), and found a weak significant correlation between GDF and VFMD ($R^2 = 0{,}120$, $p < 0.001$). Gonzalez-Hernandez et al.[26] found a significant correlation between GDF and VFMD ($p < 0.001$). Mendez-Hernandez et al.[21] observed significant moderate correlation in moderate glaucoma patients between VFMD and GDF (R2 = 0.314, $P < 0.05$). Pena-Betancor[18] et al. found significant moderate correlation between ONH Hb and VFMD ($R^2 = 0.321$, $P < 0.001$) and between ONH Hb and VF PSD ($R^2 = 0.321$, $P < 0.148$).

The pathological vascular mechanisms of glaucoma can explain our results[3,8,45–47]. Vascular dysfunction has been related to the optic nerve glaucomatous lesion[3,45,46]. The impairment of blood flow with subsequent tissue hypoxia, secondary to or independent from elevated intraocular pressure (IOP) in glaucoma, has been associated with the pathogenic mechanisms that lead to optic nerve degeneration and retinal ganglion cells loss[8,10]. Hemoglobin is the primary oxygen carrier in blood, and its concentration in tissues reflects perfusion and metabolic activity[48]. In the ONH, Hb levels are linked to the vascular supply supporting retinal ganglion cell axons and glial cells[8]. Tissues with adequate perfusion demonstrate a good level of Hb, whereas low levels occur in tissue loss[8].

Thinning of the RNFL and GCL may also influence hemoglobin levels in the optic disc[8,47]. As ganglion cell axons degenerate, metabolic demand decreases, potentially leading to reduced blood flow and, consequently, lower hemoglobin concentration[8,47]. Bidirectional relationship implies that vascular insufficiency and neurodegeneration may form a vicious cycle, exacerbating damage in glaucoma, causing RNFL and GCL thinning, and visual field loss[49–54]. The relationship between localized visual field defects and corresponding retinal nerve fiber layer loss is well established[52,55], the cause-effect relationship of retinal blood flow and neuronal dysfunction is difficult to prove[56].

In our study, the significant associations between ONH HB levels (via GDF/GIP indices) and structural (RNFLT and GCLT) and functional parameters (MD and MS) support that lower Hb correlates with RNFL and GCL loss and VF defects, reinforcing the link between perfusion and neural tissue viability[8,45,51,56]. We acknowledge that Laguna ONhE does not directly measure neural tissue but may infers its health via colorimetry analysis. Our data and cited literature support that Laguna ONhE measures a vascular biomarker (Hb) related to neural tissue integrity, offering a clinically relevant, indirect measure of glaucomatous damage. Determining the strength of structure–function relationships in glaucoma with different methods of structural and functional

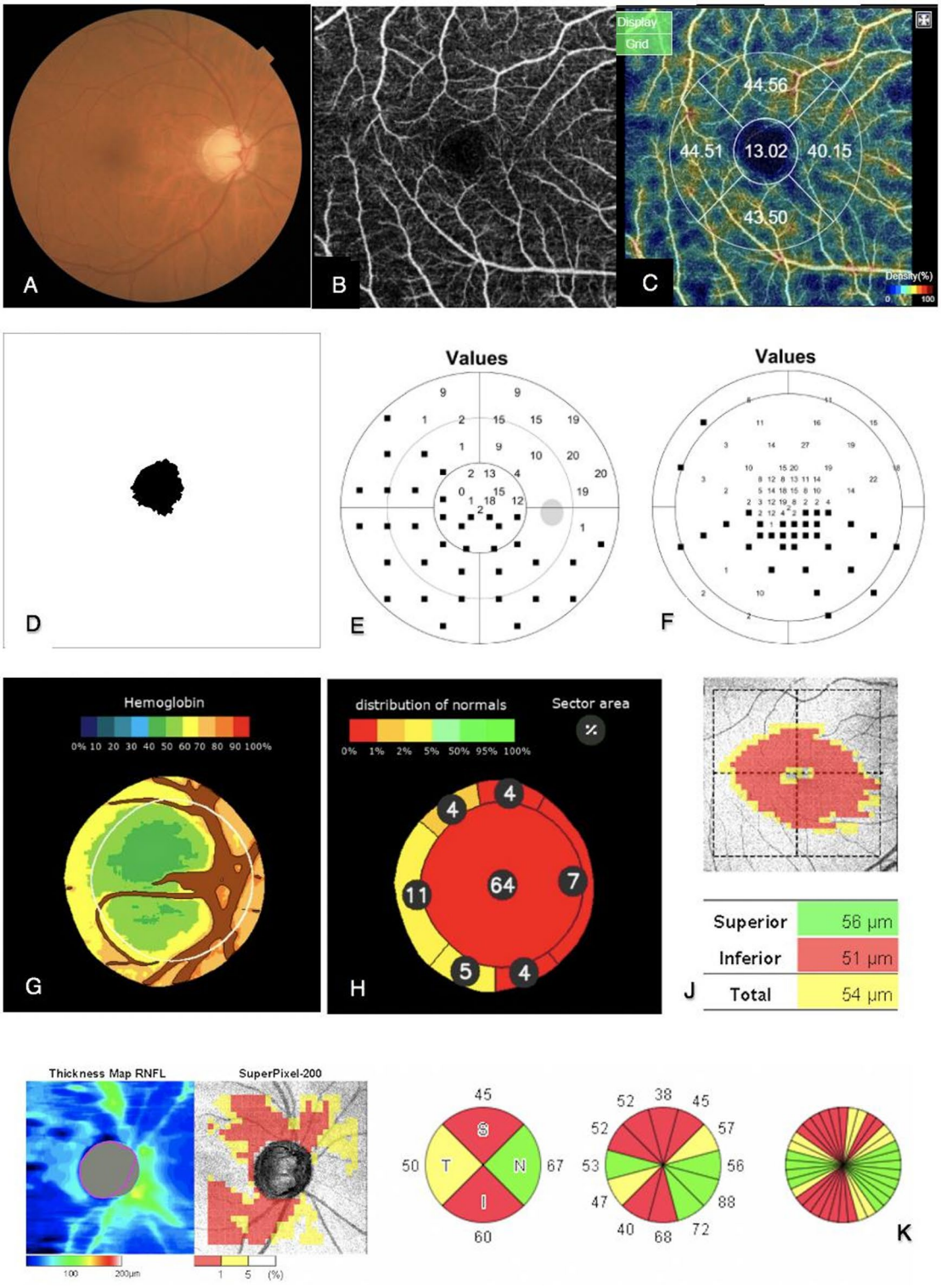

Fig. 3. Example of a patient with glaucoma. (**a**) Retinography. (**b**) OCTA – FAZ. (**c**) Macular vessel density. (**d**) FAZ area segmentation. (**e**) Octopus Visual Field G Program threshold sensitivities. (**f**) Octopus Visual Field Macular Program threshold sensitivities. (**g**) Segmentation of reference vessels and pseudo-color image of hemoglobin distribution. (**h**) Estimated sector areas as a percentage of the total area, and compared to a normal reference population. (**i**) Ganglion cell layer + inner plexiform layer thickness (GCL+). (**j**) Peripapillary retinal nerve fiber layer thickness.

assessments has significant clinical implications[29]. This not only helps in better understanding of structural and functional progression in glaucoma but also in deciding appropriate diagnostic tests during the follow-up in glaucoma patients[29]. Longitudinal studies are needed to determine whether Hb reduction precedes structural loss (suggesting vascular insufficiency as a primary insult) or follows it (due to decreased metabolic demand). Advanced multimodal imaging (e.g., combining OCTA and Laguna ONhE) could further elucidate this relationship.

Based on our findings and existing literature, we support the use of optic nerve head hemoglobin (ONH Hb) evaluation as a practical and accessible method for assessing structural damage in glaucoma, particularly due to its strong association with vascular factors[33,57,58]. The selection of a glaucoma screening approach should prioritize speed and cost-effectiveness to ensure broader population coverage[59,41]. The Laguna ONhE program delivers quantitative insights to the morphology of the optic nerve such as cup and rim area or cup-to-disc ratios by using the hemoglobin distribution in 24 sectors of the nerve[18]. Additionally, it enables the monitoring of images, which can lead to a diagnosis if notable changes, even those at the edge of normality, are detected, and facilitates the comparison of changes over the follow-up period[60,43].

This study acknowledges several limitations and characteristics that require discussion. First, the findings are specific to the population examined and cannot be generalizable to all types of glaucoma. Second, as a cross-sectional study, it does not provide insights into the prognostic significance of the GDF index. Third, the suboptimal relationship between structure and function observed in glaucoma is attributed to the varying scales of assessment and the inherent variability of both the examinations and the disease. This variability can, in certain instances, restrict the correlation between structure and function. Fourth, some participants had both eyes included in the analysis without specific statistical adjustments. While this limitation should be considered when interpreting the results, we believe such adjustments are more relevant for surgical studies, longitudinal analyses, or investigations of risk factors, rather than for cross-sectional designs. Lastly, the visual field data were not normally distributed. Although a logarithmic transformation was considered, it was not applied in the final analysis. This should be taken into account when interpreting the results.

In conclusion, our results showed significant associations between Laguna ONhE indices and both structural and functional damage in glaucoma patients obtained by OCT, OCTA, SAP and high density perimetry. Further longitudinal studies are warranted to evaluate the diagnostic performance of this technique in different types of glaucoma and as a tool for longitudinal monitoring of these patients. It remains to be demonstrated whether reduced perfusion precedes functional defects, tissue atrophy, and visual alterations.

Data availability

The datasets generated during and analysed during the current study are available from the corresponding author on reasonable request.

Received: 26 January 2025; Accepted: 21 May 2025
Published online: 01 June 2025

References

1. European Glaucoma Society Terminology and Guidelines for Glaucoma, 5th Edition. Br J Ophthalmol 105, 1–169. (2021).
2. Quigley, H. A. & Glaucoma *Lancet* **377**, 1367–1377 (2011).
3. Flammer, J. et al. The impact of ocular blood flow in glaucoma. *Prog. Retin. Eye Res.* **21**, 359–393 (2002).
4. Leske, M. C. Ocular perfusion pressure and glaucoma: clinical trial and epidemiologic findings. *Curr. Opin. Ophthalmol.* **20**, 73–78 (2009).
5. Caprioli, J. & Coleman, A. L. Blood pressure, perfusion pressure, and Glaucoma. *Am. J. Ophthalmol.* **149**, 704–712 (2010).
6. Jia, Y. et al. Quantitative OCT angiography of optic nerve head blood flow. *Biomed. Opt. Express.* **3**, 3127 (2012).
7. Tezel, G. Hypoxia-Inducible factor 1α in the glaucomatous retina and opticnerve head. *Arch. Ophthalmol.* **122**, 1348 (2004).
8. Tezel, G. et al. Hemoglobin expression and regulation in glaucoma: insights into retinal ganglion cell oxygenation. *Invest. Ophthalmol. Vis. Sci.* **51**, 907 (2010).
9. Mendez-Hernandez, C. et al. Reproducibility of optic nerve head hemoglobin measures. *J. Glaucoma*. **25**, 348–354 (2016).
10. Kur, J., Newman, E. A. & Chan-Ling, T. Cellular and physiological mechanisms underlying blood flow regulation in the retina and choroid in health and disease. *Prog. Retin. Eye Res.* **31**, 377–406 (2012).
11. Hood, D. C., Raza, A. S., de Moraes, C. G. V., Liebmann, J. M. & Ritch, R. Glaucomatous damage of the macula. *Prog. Retin. Eye Res.* **32**, 1–21 (2013).
12. Hood, D. C. et al. A Region-of-Interest approach for detecting progression of glaucomatous damage with optical coherence tomography. *JAMA Ophthalmol.* **133**, 1438 (2015).
13. The assessment of structural changes on. Optic nerve head and macula in primary open angle glaucoma and ocular hypertension. *Int. J. Ophthalmol.* https://doi.org/10.18240/ijo.2018.10.09 (2018).
14. Wu, J. H. et al. Longitudinal OCTA vessel density loss in macula and optic nerve head in healthy, glaucoma suspect and established glaucoma eyes. *Br. J. Ophthalmol.* **325746** https://doi.org/10.1136/bjo-2024-325746 (2024).
15. Hohberger, B. et al. OCT-angiography: regional reduced macula microcirculation in ocular hypertensive and pre-perimetric glaucoma patients. *PLoS ONE.* **16**, e0246469 (2021).
16. De La Gonzalez, M. et al. Measuring hemoglobin levels in the optic nerve head: comparisons with other structural and functional parameters of Glaucoma. *Invest. Ophthalmol. Vis. Sci.* **54**, 482 (2013).
17. Gonzalez-Hernandez, M., Sigut Saavedra, J. & De La Gonzalez, M. Relationship between retinal nerve Fiber layer thickness and hemoglobin present in the optic nerve head in Glaucoma. *J. Ophthalmol.* **2017**, 1–10 (2017).
18. Pena-Betancor, C. et al. Estimation of the relative amount of hemoglobin in the cup and neuroretinal rim using stereoscopic color fundus images. *Investig. Ophthalmol. Vis. Sci.* **56**, 1562–1568 (2015).
19. Medina-Mesa, E. et al. Estimating the amount of hemoglobin in the neuroretinal rim using color images and OCT. *Curr. Eye Res.* **41**, 798–805 (2016).
20. Gonzalez-Hernandez, D. et al. Segmentation of the optic nerve head based on deep learning to determine its hemoglobin content in normal and glaucomatous subjects. *J Clin. Exp. Ophthalmol* **09**, (2018).

21. Mendez-Hernandez, C., Rodriguez-Uña, I., Gonzalez-de-la Rosa, M., Arribas-Pardo, P. & Garcia-Feijoo, J. Glaucoma diagnostic capacity of optic nerve head haemoglobin measures compared with spectral domain OCT and HRT III confocal tomography. *Acta Ophthalmol.* **94**, 697–704 (2016).
22. Rocha, J. A. G. et al. Optic nerve head hemoglobin levels in glaucoma: A structural and functional correlation study. *J. Ophthalmol.* **2021**, 1–8 (2021).
23. Lima, V. C. et al. A comparison between microperimetry and standard achromatic perimetry of the central visual field in eyes with glaucomatous paracentral visual-field defects. *Br. J. Ophthalmol.* **94**, 64–67 (2010).
24. Lin, Y. et al. Spatial positional relationship between macular superficial vessel density and ganglion cell-inner plexiform layer thickness in primary angle closure glaucoma. *Int. Ophthalmol.* **42**, 103–112 (2022).
25. Lin, A., Fang, D., Li, C., Cheung, C. Y. & Chen, H. Improved automated foveal avascular zone measurement in cirrus optical coherence tomography angiography using the level sets macro. *Trans. Vis. Sci. Tech.* **9**, 20 (2020).
26. Gonzalez-Hernandez, M. et al. Fully Automated Colorimetric Analysis of the Optic Nerve Aided by Deep Learning and Its Association with Perimetry and OCT for the Study of Glaucoma. *JCM* **10**, 3231 (2021).
27. Gonzalez-Hernandez, M., Gonzalez-Hernandez, D. & Perez-Barbudo, D. Gonzalez de La Rosa, M. Optic disc area frequency distribution in a large sample of retinographic images. *BMJ Open. Ophth*. **7**, e000972 (2022).
28. Jerez-Olivera, E., Gonzalez-Hernandez, M. & Gonzalez-Hernandez, D. Gonzalez de La Rosa, M. Estimation of normal and glaucomatous optic nerve morphology from perfusion. *BMJ Open. Ophth*. **10**, e002024 (2025).
29. Medeiros, F. A., Zangwill, L. M., Bowd, C., Mansouri, K. & Weinreb, R. N. The structure and function relationship in glaucoma: implications for detection of progression and measurement of rates of change. *Invest. Ophthalmol. Vis. Sci.* **53**, 6939 (2012).
30. Malik, R., Swanson, W. H. & Garway-Heath, D. F. Structure–function relationship' in glaucoma: past thinking and current concepts. *Clin. Exper Ophthalmol.* **40**, 369–380 (2012).
31. Nishida, T. et al. Association of initial optical coherence tomography angiography vessel density loss with faster visual field loss in Glaucoma. *JAMA Ophthalmol.* **140**, 319 (2022).
32. Hirasawa, K. et al. Discrepancy in loss of macular perfusion density and ganglion cell layer thickness in early Glaucoma. *Am. J. Ophthalmol.* **221**, 39–47 (2021).
33. Wang, R. et al. Changes of macular blood flow and structure in acute primary angle closure glaucoma. *Int. Ophthalmol.* **42**, 3789–3801 (2022).
34. Kwon, J., Choi, J., Shin, J. W., Lee, J. & Kook, M. S. Glaucoma diagnostic capabilities of foveal avascular zone parameters using optical coherence tomography angiography according to visual field defect location. *J. Glaucoma*. **26**, 1120–1129 (2017).
35. Bussel, I. I., Wollstein, G. & Schuman, J. S. OCT for glaucoma diagnosis, screening and detection of glaucoma progression. *Br. J. Ophthalmol.* **98**, ii15–ii19 (2014).
36. Suh, M. H. et al. Optical coherence tomography angiography vessel density in glaucomatous eyes with focal Lamina cribrosa defects. *Ophthalmology* **123**, 2309–2317 (2016).
37. Rauscher, F. M., Sekhon, N., Feuer, W. J. & Budenz, D. L. Myopia affects retinal nerve Fiber layer measurements as determined by optical coherence tomography. *J. Glaucoma*. **18**, 501–505 (2009).
38. Kim, N. R. et al. Factors associated with false positives in retinal nerve Fiber layer color codes from Spectral-Domain optical coherence tomography. *Ophthalmology* **118**, 1774–1781 (2011).
39. Chong, G. T. & Lee, R. K. Glaucoma versus red disease: imaging and glaucoma diagnosis. *Curr. Opin. Ophthalmol.* **23**, 79–88 (2012).
40. Tham, Y. C. et al. Global prevalence of Glaucoma and projections of Glaucoma burden through 2040. *Ophthalmology* **121**, 2081–2090 (2014).
41. Olson, J. et al. Improving the economic value of photographic screening for optical coherence tomography-detectable macular oedema: a prospective, multicentre, UK study. *Health Technol. Assessment* **17**, (2013).
42. Meneses, L. S. D., Ciarlini, L. R., Ayub, G., Vasconcellos, J. P. C. & Costa, V. P. Discrimination between healthy eyes and those with mild Glaucoma damage using hemoglobin measurements of the optic nerve head. *J. Glaucoma*. **31**, 567–573 (2022).
43. Rocha, J. A. G. et al. Assessment of structural progression in Glaucoma through automated optic nerve head hemoglobin measurements. *J. Glaucoma*. **34**, 182–188 (2025).
44. Mendez-Hernandez, C. et al. Diagnostic validity of optic nerve head colorimetric assessment and optical coherence tomography angiography in patients with glaucoma. *Br. J. Ophthalmol.* **105**, 957–963 (2021).
45. Flammer, J., Haefliger, I. O., & Resink, T. Vascular dysregulation: A principal risk factor for glaucomatous damage?? *J. Glaucoma*. **8**, 212–219 (1999).
46. Flammer, J., Konieczka, K. & Flammer, A. J. The primary vascular dysregulation syndrome: implications for eye diseases. *EPMA J.* **4**, 14 (2013).
47. Hayreh, S. S. Blood flow in the optic nerve head and factors that May influence it. *Prog. Retin. Eye Res.* **20**, 595–624 (2001).
48. Gell, D. A. Structure and function of haemoglobins. *Blood Cells Molecules Dis.* **70**, 13–42 (2018).
49. Alarcon-Martinez, L. et al. Neurovascular dysfunction in glaucoma. *Prog. Retin. Eye Res.* **97**, 101217 (2023).
50. Tezel, G. Multifactorial pathogenic processes of retinal ganglion cell degeneration in Glaucoma towards Multi-Target strategies for broader treatment effects. *Cells* **10**, 1372 (2021).
51. Wang, X. et al. The Association between Vascular Abnormalities and Glaucoma—What Comes First? *IJMS* **24**, 13211 (2023).
52. Horn, F. K. et al. Correlation between local glaucomatous visual field defects and loss of nerve Fiber layer thickness measured with polarimetry and spectral domain OCT. *Invest. Ophthalmol. Vis. Sci.* **50**, 1971 (2009).
53. Casado, A. et al. Topographic correlation and asymmetry analysis of ganglion cell layer thinning and the retinal nerve fiber layer with localized visual field defects. *PLoS ONE*. **14**, e0222347 (2019).
54. Kim, J. S. et al. Topographic correlation between macular superficial microvessel density and ganglion cell-inner plexiform layer thickness in glaucoma-suspect and early normal-tension glaucoma. *Br. J. Ophthalmol.* **104**, 104–109 (2020).
55. Horn, F. K., Mardin, C. Y., & Viestenz, A. Association between localized visual field losses and thickness deviation of the nerve Fiber layer in Glaucoma. *J. Glaucoma*. **14**, 419–425 (2005).
56. Zhou, W. & Sabel, B. A. Vascular dysregulation in glaucoma: retinal vasoconstriction and normal neurovascular coupling in altitudinal visual field defects. *EPMA J.* **14**, 87–99 (2023).
57. Nakazawa, T. Ocular blood flow and influencing factors for Glaucoma. *Asia-Pacific J. Ophthalmol.* **5**, 38–44 (2016).
58. Pasquale, L. R. Vascular and autonomic dysregulation in primary open-angle glaucoma. *Curr. Opin. Ophthalmol.* **27**, 94–101 (2016).
59. Mendez-Hernandez, C., Gutierrez-Diaz, E., Pazos, M., Gimenez-Gomez, R. & Pinazo-Duran, M. D. Agreement between five experts and the Laguna ONhE automatic colourimetric application interpreting the glaucomatous aspect of the optic nerve. *JCM* **12**, 5485 (2023).
60. Gonzalez-Hernandez, M. et al. Glaucoma Incidence and Progression in Diabetics: The Canary Islands Study Using the Laguna ONhE Application. *JCM* **11**, 7294 (2022).

Author contributions

Gustavo Coelho Caiado conceived and designed the study, performed data acquisition, conducted data analysis and interpretation, and prepared the manuscript. Gustavo Albrecht Samico and Gilvan Vilarinho da Silva Filho

contributed to data acquisition and assisted with data analysis. Sérgio Henrique Teixeira, Tiago dos Santos Prata, Carolina Pelegrini Barbosa Gracitelli and Augusto Paranhos Jr participated in data interpretation and provided critical revisions to the manuscript. Carolina Pelegrini Barbosa Gracitelli and Augusto Paranhos Jr supported experimental design, data acquisition, and contributed to the discussion of results. Augusto Paranhos Jr supervised the research, coordinated the project, and handled manuscript submission and correspondence. All authors reviewed, edited, and approved the final version of the manuscript. All authors have agreed both to be personally accountable for the author's own contributions and to ensure that questions related to the accuracy or integrity of any part of the work, even ones in which the author was not personally involved, are appropriately investigated, resolved, and the resolution documented in the literature.

Declarations

Competing interests
The authors declare no competing interests.

Additional information
Correspondence and requests for materials should be addressed to A.P.

Reprints and permissions information is available at www.nature.com/reprints.

Publisher's note Springer Nature remains neutral with regard to jurisdictional claims in published maps and institutional affiliations.

Open Access This article is licensed under a Creative Commons Attribution-NonCommercial-NoDerivatives 4.0 International License, which permits any non-commercial use, sharing, distribution and reproduction in any medium or format, as long as you give appropriate credit to the original author(s) and the source, provide a link to the Creative Commons licence, and indicate if you modified the licensed material. You do not have permission under this licence to share adapted material derived from this article or parts of it. The images or other third party material in this article are included in the article's Creative Commons licence, unless indicated otherwise in a credit line to the material. If material is not included in the article's Creative Commons licence and your intended use is not permitted by statutory regulation or exceeds the permitted use, you will need to obtain permission directly from the copyright holder. To view a copy of this licence, visit http://creativecommons.org/licenses/by-nc-nd/4.0/.

© The Author(s) 2025